

Flow boiling of a new low-GWP refrigerant inside a single square cross section microchannel

S Bortolin and D Del Col

Dipartimento di Ingegneria Industriale, Università degli Studi di Padova
Via Venezia 1, I-35131 Padova, Italy

E-mail: stefano.bortolin@unipd.it

Abstract. In this work new experimental heat transfer coefficients measured during flow boiling of HFO-1234ze(E) in a horizontally-assembled square cross section microchannel having an hydraulic diameter of 1.23 mm are presented. The test runs have been performed at around 30°C saturation temperature, correspondent to 5.8 bar, with mass flux ranging between 300 kg m⁻² s⁻¹ and 500 kg m⁻² s⁻¹. As a peculiar characteristic of the present technique, the heat transfer coefficient is not measured by imposing the heat flux; instead, the boiling process is governed by controlling the inlet temperature of the heating secondary fluid. On this regard the present data is new and original since the large majority of data in the literature is taken by means of Joule effect heating. The heat transfer coefficients are compared against two predicting models available in the literature. Finally, the local heat transfer coefficients measured during flow boiling of R1234ze(E) inside the square cross section microchannel are compared against the values measured with the same refrigerant in a 0.96 mm diameter circular microchannel, with same surface roughness, with the aim of investigating the effect of channel shape on the heat transfer process.

1. Introduction

During the last years, flow boiling heat transfer inside microchannels has received increasing attention due to the rapid advances in microfabrication technology along with increasing demand for space saving and energy conservation in many applications. Although miniaturization offers many benefits, however, flow boiling in micro-devices itself involves a very complex combination of thermophysical processes which are still far from being entirely understood. Differently from single-phase flow heat transfer, the current knowledge of flow boiling heat transfer in macroscale cannot be extended without modifications to microscale, where bubble confinement plays a more relevant role with the decreasing of the channel size. In two-phase microchannel flow, capillary (surface tension) forces become predominant over gravity force, thus impeding stratification of liquid. As reported by Thome *et al.* [1], bubble flow, slug flow, annular flow and mist flow are the primary flow regimes observed in microchannels. For evaporating flow, the zone with bubbles smaller than channel diameter is very short as bubbles grow to the channel size very quickly. Chen *et al.* [2] investigated flow patterns in four circular tubes with internal diameters of 1.10, 2.01, 2.88 and 4.26 mm. The experiments were conducted in vertical upward two-phase flow using R134a as working fluid at 6, 10 and 14 bar pressure. The flow characteristics in the 2.88 and 4.26 mm tubes are similar to those typically observed in normal size tubes, while the 1.10 mm and the 2.01 mm tubes exhibit small tube characteristics. Dispersed bubble, bubbly, confined bubble, slug, churn and annular are the flow regimes observed by those authors inside the 1.1 mm diameter channel. The confined bubble flow appears in the 1.10 mm tube at all experimental pressure, suggesting that the surface tension becomes



the dominant force. Tibirić and Ribatsky [3] presented flow pattern and bubble departure characteristics during R134a and R245fa flow boiling in a 0.4 mm circular horizontal channel at mass velocity ranging from 100 to 900 kg m⁻²s⁻¹ and heat flux up to 226 kW m⁻². Four main flow patterns were observed (bubble, slug, annular and dryout) and the absence of the stratified flow is remarked.

In spite of the large number of papers published in the flow boiling area, many aspects still need to be better explained in order to provide a full understanding of local two-phase flow boiling characteristics in microchannels. Such knowledge is essential to develop more reliable prediction methods that can be used for designing new high-performance microchannel evaporators. The relative importance of nucleate boiling, thin film evaporation and convective boiling in the individual flow patterns, that are characteristics to a microchannel flow, is still unclear. Some recent studies have put some light on the main heat transfer mechanism. However, additional innovative studies are necessary to investigate local phenomena (Tibirić and Ribatski [4]). Some experimental studies show that the heat transfer coefficients obtained during vaporization in microchannels are not a function of vapor quality nor mass velocity (in contrast with the macro-channel trend), but they are a function of heat flux and saturation pressure, concluding that flow boiling in small channels is dominated by nucleate boiling (Bao *et al.* [5], Tran *et al.* [6]). Other experimental studies demonstrate that the heat transfer coefficient also depends on vapor quality and mass velocity (Yan and Lin [7], Lin *et al.* [8], Ong *et al.* [9]). Thome [10] suggests that during slug flow, nucleate boiling is completely suppressed and heat is transfer primarily by conduction through the thin evaporating film surrounding the elongated bubbles. According to the authors, the strong dependency of the boiling heat transfer coefficients on the heat flux is mechanistically explainable by the thin-film evaporation process and the cyclic heat transfer process occurring in elongated bubble flows.

Generally speaking, most of the boiling studies were performed in multiport rectangular channels. In single channels, studies were generally performed inside circular cross section microchannels with halocarbon refrigerants and fluid temperatures typical of the room ambient. Very few works deal with boiling in non-circular single-channels. In the great majority of cases, the fluid evaporation is obtained by applying electric current directly to the channel. With regard to the test fluids, most studies have been performed with HFC refrigerants which have relatively large values of GWP, but recent development efforts have been initiated to investigate halogenated olefins as possible refrigerants, with fluorinated propene isomers, in particular, having emerged as possible solutions. R1234ze(E), which has a 100-years horizon global warming potential less than 1 (IPCC [11]), seems to be suitable to substitute R134a in refrigeration applications.

Tibirić *et al.* [12] obtained flow boiling experimental data for the refrigerant R1234ze(E) in two horizontal stainless steel circular channels with diameter of 1.0 and 2.2 mm. The experimental campaign includes mass velocities ranging from 50 to 1500 kg m⁻² s⁻¹, heat fluxes from 10 to 300 kW m⁻² and saturation temperature of 25°C, 31°C and 35°C. R1234ze(E) demonstrated similar thermal performance with respect to R134a when running at similar conditions. Flow pattern characterization was performed, indicating that for both channel diameters microscale phenomena have already shown to be important. With regard to the heat transfer, they found that an increase in mass velocity or in vapor quality causes an increase in heat transfer coefficient at constant heat flux.

Del Col *et al.* [13] investigated the flow boiling process of R1234yf and R1234ze(E) inside a horizontal single circular microchannel with 0.96 mm internal diameter at 31°C saturation temperature. During the tests, the heat flux is not imposed, but it is transferred from a secondary fluid (water) to the evaporating refrigerant. The heat transfer coefficient shows to be highly dependent on the heat flux while it decreases with vapor quality when all the others parameters are constant. The mass velocity was found to have a minor effect. From the comparison between the tested refrigerants, the heat transfer coefficients of R1234yf are around 20% higher than those of R1234ze(E) and this may be related to the different reduced pressure of the fluids.

Recently, Vakili-Farahani *et al.* [14] carried out upward flow boiling experiments in a flat aluminum extruded multiport tube, which is composed of 7 parallel rectangular channels (1.1 mm x 2.1 mm) with hydraulic diameter of 1.4 mm. Two refrigerants, R245fa and R1234ze(E) were tested. A new hot water heating technique that accounts for either uniform or nonuniform local heat flux distribution along the channel was developed to obtain and reduce the data. Effects of heat flux, mass

flux, vapor quality, and saturation temperature on flow boiling heat transfer in multiport tubes were considered. Once saturated boiling begins, the heat transfer coefficient profile remains either rather flat with vapor quality. Moreover, the heat transfer coefficient increases with increase of saturation temperature, heat flux and mass flux.

With reference to microchannel flow boiling databases in the open literature, it appears that most experimentalists use electrical heating. Very few researchers took data of flow boiling of a refrigerant against a secondary fluid, and this data when available refers to multiport microchannels, instead of a single microchannel. However, there are many applications where the heat flux is a dependent variable, as it happens when it is transferred from a secondary fluid. This is the case of automotive and domestic air conditioning, where the heat is removed from a secondary fluid (air).

Starting from this background, in this work new experimental heat transfer coefficients measured during flow boiling of HFO-1234ze(E) in a square cross section microchannel having an hydraulic diameter of 1.23 mm are presented. As a peculiar characteristic of the present technique, the heat transfer coefficient is not measured by imposing the heat flux; instead, the boiling process is governed by controlling the inlet temperature of the heating secondary fluid. The flow boiling data taken in the present test section is discussed, with particular regard to the effect of heat flux, mass velocity and vapor quality.

2. Experimental apparatus

The test rig used for the experimental tests is depicted in figure 1. It consists of the primary (refrigerant) loop and of two auxiliary loops: the hot water loop to promote boiling and the cold water loop to control the refrigerant condensation after the test section. The subcooled refrigerant from the condenser is sent through a filter drier into an independently controlled gear pump, which is magnetically coupled to a variable speed electric motor. During flow boiling measurements, the fluid is pumped through the Coriolis-effect mass flow meter into the test section as a subcooled liquid. The refrigerant enters the test section, which is made of two counter-flow heat exchangers. The first one (pre-sector) is used to achieve the desired inlet condition and the second one is the actual measuring sector. The refrigerant enters the test section, which is made of two counter-flow heat exchangers. The first one (pre-sector) is used to achieve the desired inlet condition and the second one is the actual measuring sector.

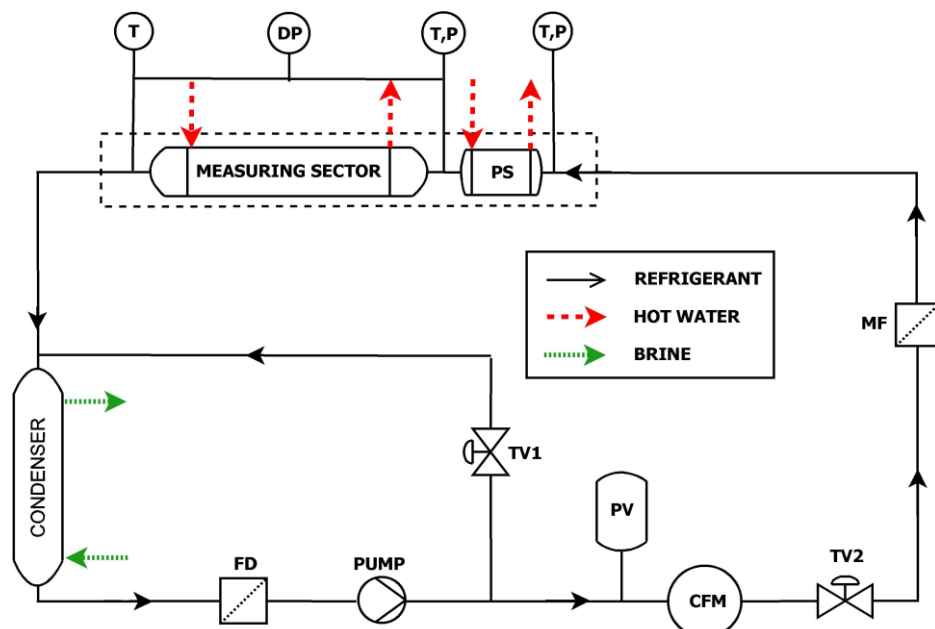


Figure 1. Experimental test rig. (FD=filter drier, PV=pressure vessel, CFM=Coriolis-effect mass flow meter, TV=throttling valve, MF=mechanical filter, PS=pre-sector, P=pressure transducer, T=temperature transducer, DP=differential pressure transducer).

The pressure is gauged through two digital pressure transducers, connected to manometric taps to measure the fluid pressure upstream and downstream of the test tube. Two refrigerated thermal baths are used in the flow boiling tests. The first one provides the water entering the measuring sector and the pre-sector at a desired temperature and the other one provides the coolant for the condenser. When necessary, the water entering the pre-sector and the measuring sector can be maintained at different temperatures through an electric heater installed downstream of the thermal bath. The water flow rates, in the pre-sector and in the measuring sector, are measured by means of two Coriolis-effect mass flow meters and the total temperature difference of water across both sectors is measured with four copper-constantan thermocouples.

A sketch of the microchannel test section is reported in figure 2. The channel is obtained from a copper rod and has a square cross section with 1.18 mm side length. Each corner has a curvature radius equal to 0.15 mm, which leads to a hydraulic diameter equal to 1.23 mm. The internal surface roughness of the copper channel has been measured with the digital surface roughness machine ZEISS-TSK Surfcom 1400A. The measurements have been performed at different positions. The mean roughness Ra , as defined by the ISO 4287:1997, ranges between 0.80 μm and 1.32 μm , with a mean value equal to 1.02 μm . Figure 2 also shows the passage for the water. The geometry has been designed with the aim of increasing the external heat transfer area and thus decreasing the external heat transfer resistance. This complex flow passage causes an internal local mixing of the water and thus high heat transfer coefficients by changing continuously the flow direction and disturbing the boundary layer. During the fabrication process of the test section, the water channel in the copper is externally contained by means of a covering made with epoxy resin. The thermocouples embedded in the wall are installed in 0.6 mm diameter cylindrical holes, machined 0.5 mm away from the internal tube surface. The measuring sector is 225 mm long and is equipped with a large number of thermocouples (19 in the water, 45 in the wall). Position of thermocouples in the wall and in the water is shown in figure 2. The measuring sector is thermally separated from the pre-sector and the exit tube through stainless steel capillary tubes (adiabatic segments).

The present test tube, with the described water channel, allows the measurement of local “quasi-mixing cup” temperatures of the water at low flow rates directly in the external annular space, permitting evaluation of the local heat flux from the water temperature gradient. In particular, water thermocouples wires are fixed in the cover made with epoxy resin that surrounds the water channel. In this way the water thermocouples are not in contact with the copper block, avoiding undesired temperature gradients. Secondly, the present design of the test section allows to embed several thermocouples in the tube without passing them through the water flow and thus preventing also the wall thermocouple wires from being exposed to severe temperature gradients.

3. Data reduction

In the present setup, the heat flux is determined from the temperature profile of the secondary fluid in the measuring sector. The wall temperature is measured by means of thermocouples embedded in the copper tube. Since the wall thermocouples are installed 0.5 mm far from the internal tube surface, a correction is required for the calculation of the heat transfer coefficient due to the distance between the thermocouple and the inner tube surface. This correction is accounted for by calculating the conductive thermal resistance of the copper between inner tube surface and wall thermocouple.

The saturation temperature is directly measured in the adiabatic segments at the inlet and outlet of the measuring sector (figure 1), by means of two T-type thermocouples soldered to the stainless steel adiabatic capillary tubes. The presence of both temperature and pressure sensors at the inlet of the measuring sector allows a double check of the saturation temperatures.

Figure 3 displays the refrigerant, wall and water temperature measurements along the measuring sector during flow boiling of R1234ze(E) at mass velocity $G = 300 \text{ kg m}^{-2} \text{ s}^{-1}$. The refrigerant enters the test channel at 30.2°C saturation temperature (corresponding to 5.8 bar saturation pressure) with about 5 K subcooling. At the exit, saturation temperature is decreased by 1.3 K due to pressure drop.

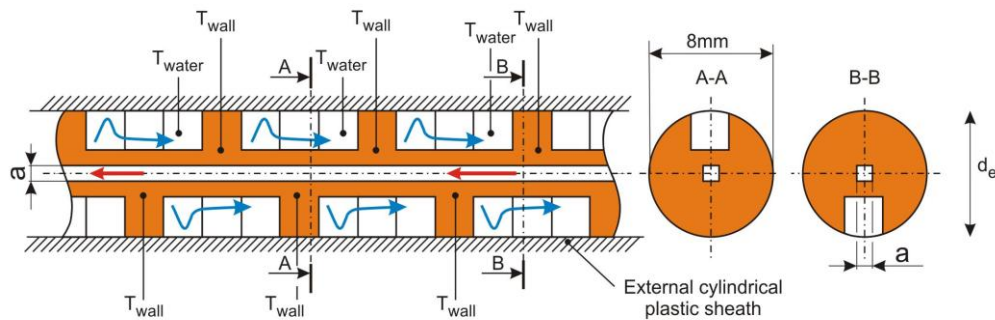


Figure 2. Detailed sketch of the test section: geometry of the water flow passage.

The water enters from the opposite side of the test tube at 37.2°C and its temperature decreases due to the heat transfer to the boiling refrigerant. As the vaporization proceeds, the wall temperature increases uniformly up to the end of the test section. Figure 3 also shows the standard deviation of the temperature readings in the wall: each temperature measurement is the average value of fifty readings taken in fifty seconds and standard deviations are pretty much the same in all the channel. It should be mentioned that, during experimental tests, when dryout takes place, a great increase of the wall temperature standard deviation is found just at the location where the heat transfer starts to decrease due to the thermal crisis. The standard deviation of the fifty temperature readings goes back to the initial values in the superheated vapor zone. This trend was previously detected by Del Col *et al.* [15] and it is related to the dryout of the film adjacent to the heated wall and the temperature fluctuation is the symptom of an oscillating drying process of the film at the wall. It is worth noting the relevance of such a criterion for the determination of the critical quality in the channel when the heat flux is not imposed. During tests with electrical heating, when the critical conditions occur, an abrupt change in the wall temperature is evident. When vaporizing by means of a secondary fluid, still there is a temperature change in the wall, but it is limited by the temperature of the secondary fluid. Only the data points characterized by vaporization prior to onset of dryout are considered in the present paper.

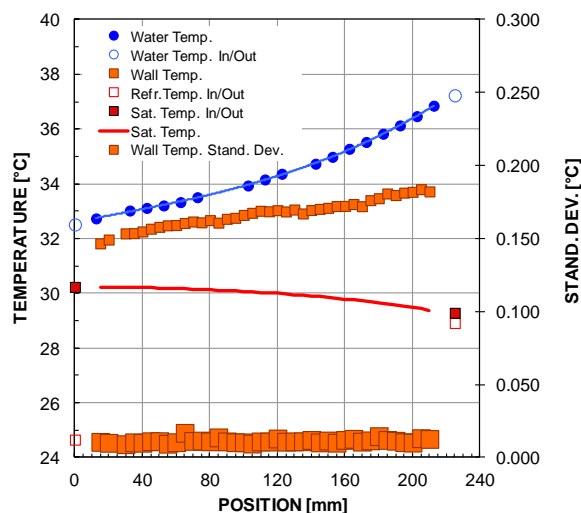


Figure 3. Water, wall and saturation temperature at $G = 400 \text{ kg m}^{-2} \text{ s}^{-1}$. The big square dots represent the standard deviation of the wall temperature recording.

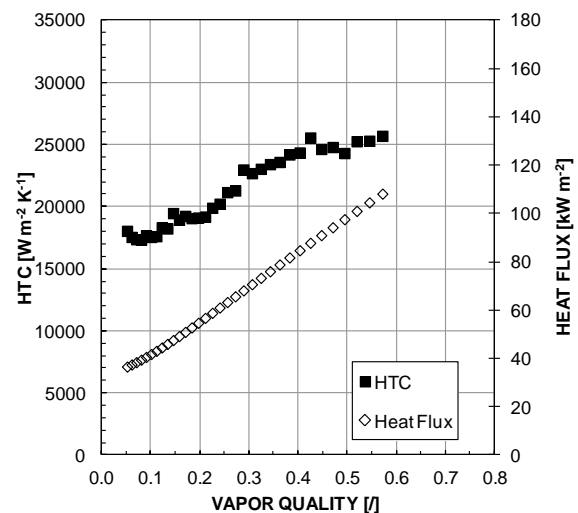


Figure 4. R1234ze(E) flow boiling test at $G = 400 \text{ kg m}^{-2} \text{ s}^{-1}$: heat transfer coefficient and heat flux versus vapor quality.

3.1. Heat flux

Since the heat flux q' is not directly fixed here, it must be obtained indirectly, from the slope of the secondary fluid temperature profile:

$$q' = \dot{m}_w \cdot c_{p,w} \cdot \frac{1}{p} \frac{dT_w}{dz} \quad (1)$$

where z is the axial coordinate along the tube, dT_w/dz is the derivative of the water temperature along z , \dot{m}_w is the water mass flow rate, $c_{p,w}$ is the water specific heat capacity and p is the channel perimeter. In the calculation, a polynomial function is used to interpolate the water temperature profile along the channel. Two different independent procedures have been adopted for the determination of the fitting polynomial degree of the water temperature and thus the calculation of the heat flux (equation 1). The first criterion, dubbed as physical, is based on the assumption that all the calculated values by the polynomial interpolation of the water temperatures should be below ± 0.05 K with respect to the experimental values, and 68% of the predicted values should be inside the ± 0.03 K prediction boundary. Beside this, a statistical method based on the choice of the simplest fitting polynomial has been used. This statistic approach uses the R^2 statistic parameter, and adjusts it on the basis of the residual degrees of freedom: this is the reason of the name R^2_{adj} (Rawlings *et al.* [16]). The polynomial degree is the one that can satisfy both criteria.

3.2. Saturation temperature

The fluid temperature is directly measured by means of adiabatic segments only at inlet and outlet of the test tube. Nevertheless the local saturation temperature can be determined from the pressure profile along the channel. When the pressure is measured at inlet and outlet, as in the present case, a linear variation is usually assumed in the channel. However, during vaporization, the vapor quality changes along the microchannel and therefore the pressure gradient varies in the measuring sector; for this reason, a linear interpolation of the saturation temperature between inlet and outlet may lead to errors in the determination of the heat transfer coefficient. Instead, in the present work, the pressure profile inside the microchannel is calculated by implementing the Del Col *et al.* [17] two-phase pressure gradient correlation and then integrating the calculated pressure gradient over the total length: the resulting value is corrected by an empirical coefficient to match the total pressure drop to the value measured by the differential pressure transducer. Once the pressure profile is known, the local saturation temperature can be determined. In figure 3 the saturation temperature profile is plotted with a solid line.

3.3. Heat transfer coefficient and vapor quality

The local heat transfer coefficient α inside the microchannel is obtained as the ratio of heat flux q' to temperature difference:

$$\alpha = \frac{q'}{(T_{wall} - T_{sat})} \quad (2)$$

where the saturation temperature T_{sat} is obtained from pressure measurements. The measured saturation temperature at the outlet can be compared with the saturation temperature obtained from the pressure, provided that no local superheating occurs.

The vapor quality x at any axial position z is obtained from:

$$x = \frac{q - \dot{m}_r \cdot (h_{SL} - h_{sub})}{\dot{m}_r \cdot h_{LG}} \quad (3)$$

as a function of the total heat flow rate q up to that location, the specific enthalpy of saturated liquid (h_{SL}), the specific enthalpy of the subcooled liquid (h_{sub}), the latent heat (h_{LG}) and the refrigerant mass flow rate \dot{m}_{ref} . The enthalpy of the subcooled refrigerant is determined from the inlet pressure and

temperature, while the total heat flow rate transferred to the refrigerant is obtained by integrating the local heat flux q' from 0 (refrigerant inlet) to z .

3.4. Axial conduction

Given the measurement of the wall temperature along the channel, it is possible to calculate the contribution of the axial conduction in the copper wall. The effect of axial conduction on the heat transfer coefficient can be determined from an energy balance at the wall: this allows to determine the actual heat flux to be used in the evaluation of the heat transfer coefficient. The heat transfer coefficient is corrected by the same amount as the heat flux, being fixed the measured values of wall and saturation temperature. The correction for axial conduction does not significantly affect the values of heat flux and heat transfer coefficient.

4. Flow boiling results

Flow boiling tests have been performed with R1234ze(E) at mass velocity ranging between 300 and 500 kg m⁻² s⁻¹, at a saturation temperature around 30°C in the present 1.23 mm hydraulic diameter square cross section channel. During the test runs, only mass velocities and inlet fluid temperatures can be fixed; thus the heat flux varies along the process and this complicates the comparison of the present tests to the ones obtained with electrical heating. Wall and water temperature profiles during flow boiling process at $G = 400$ kg m⁻² s⁻¹ are illustrated in figure 4. Since refrigerant and water flow in counter-current, the heat flux usually increases along the channel in the refrigerant flow direction. Figure 4 reports heat flux, vapor quality and heat transfer coefficient. The heat flux and the heat transfer coefficient increase with vapor quality. No dryout is reached during the test run. All the data points reported in the present chapter were taken after steady state conditions were reached by at least ten minutes. Furthermore experimental data refer to boiling conditions before the dryout. Test runs are performed with decreasing heat flux, to make sure that all nucleation sites are activated.

4.1. Heat flux

In this work the heat flux is not electrically imposed: the controlled parameters are the inlet temperature and the mass flow rate of the secondary fluid. As a consequence, for each test run, not only the heat transfer coefficient and the vapor quality vary along the channel but also the heat flux is a dependent variable (figure 4). Therefore, with the present technique, it is impossible to get the heat transfer coefficient variation with vapor quality in one test run as reported in literature studies using electric heating. In order to explore the effects of heat flux and vapor quality on the heat transfer coefficient, several tests were made at constant refrigerant mass velocity and varying the inlet water conditions (mass flux and temperature). A further data processing is then required to investigate the effects of vapor quality, mass velocity and heat flux on the heat transfer coefficient.

The effect of heat flux on the heat transfer coefficient can be better understood in figure 5 where the heat transfer data has been filtered at constant quality $x = 0.2$ for three different mass velocities. The data points show a clear dependence of the heat transfer coefficient on the heat flux. The rising heat transfer coefficients with heat flux in the saturated region conform with the results observed by many authors (Lazarek and Black [18], Ong and Thome [19], Del Col *et al.* [20]).

4.2. Mass velocity and vapor quality

The effect of mass velocity on the heat transfer coefficient can be found in figure 5. It can be seen that at a given heat flux, the corresponding heat transfer coefficients are independent of mass velocity. Such behavior has been confirmed by other experiments (Shiferaw *et al.* [21] and Maqbool *et al.* [22]).

By processing data at constant heat flux, it is possible to get information on the influence of vapor quality. Figure 6 shows the experimental trend of heat transfer coefficient at 300 and 400 kg m⁻² s⁻¹ mass velocity. Two different values of heat flux are considered. The heat transfer coefficient is pretty constant with vapor quality for both conditions.

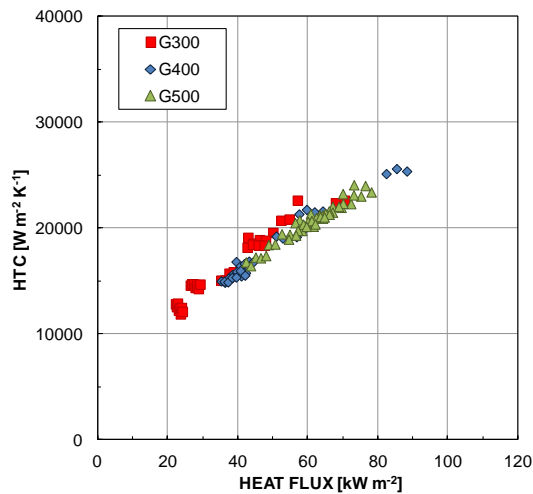


Figure 5. Local heat transfer coefficient versus heat flux at constant vapor quality $x = 0.2$.

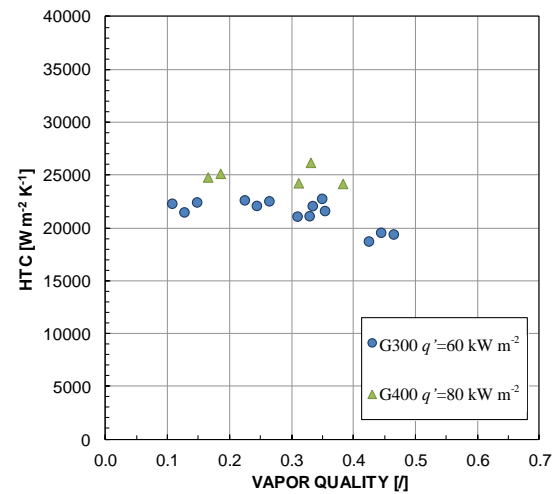


Figure 6. Local heat transfer coefficient versus vapor quality at two different values of heat flux q' and mass flux G [$\text{kg m}^{-2} \text{s}^{-1}$].

4.3. Effect of channel shape

In figure 7, the present data is compared with R1234ze(E) flow boiling measurements by Del Col *et al.* [13] in a round channel. The test section was a copper cold drawn tube of internal diameter 0.96 mm, and roughness $Ra = 1.3 \mu\text{m}$. Del Col *et al.* [13] data is taken at mass velocity ranging between 300 and 500 $\text{kg m}^{-2} \text{s}^{-1}$, heat flux from 20 to 100 kW m^{-2} , 0.2 quality and 30°C saturation temperature. The experimental conditions are similar to the ones tested by the present authors. From the graph in figure 7, it is clear that the heat transfer coefficients in the square channel are higher than those obtained in the circular channel. Since flow visualization inside the square channel is not possible, only an attempt to give a physical explanation of such behavior can be made.

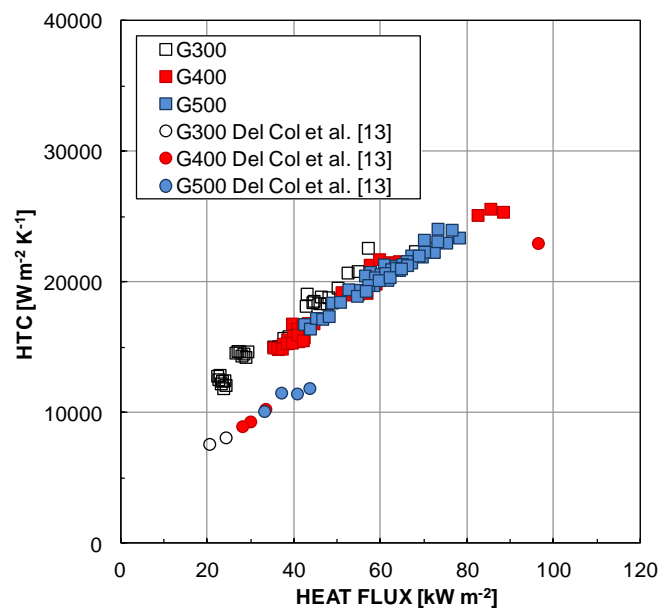


Figure 7. Comparison between the heat transfer coefficients obtained inside the present square channel and the data by Del Col *et al.* [13] inside a 0.96 mm circular channel at 0.2 vapor quality.

In the work by Tibirić and Ribatski [3] it is reported that bubbles can detach from the wall with diameters smaller than the tube diameter and the authors observed bubble active sites for all flow patterns, also in the slug flow regime. They found that, according to the heat flux level over the tube surface, the number of nucleation sites increases. For lower heat flux conditions, one nucleation site is possible but increasing the heat flux, multiple nucleation sites become active. Furthermore, nucleation sites can also be active over all vapor quality range, depending on the level of the applied heat flux and the presence of liquid in contact with the wall.

The surface tension in a square channel is known to push the liquid towards the corners of the channel, leading to a thinner liquid film on the flat sides (Bortolin *et al.* [23]). Starting from the visualizations by Tibirić and Ribatski [3] it can be argued that the heat transfer coefficient enhancement in the square channel could be due to the presence of several active nucleation sites at the corners of the channel, where the liquid is pulled by surface tension. However, more investigation is needed to confirm such hypothesis. Also, it is worth mentioning that the diameters of the square and the circular channels are not exactly the same.

5. Comparison with the models

More than 650 data points have been collected during the present experimental campaign. Vapor quality varies between 0.05 and 0.7, mass velocity between 300 and 500 kg m⁻² s⁻¹, while the heat flux ranges from 20 to 140 kW m⁻². The present database has been compared against two models available in the open literature: the model by Lazarek and Black [18] and the model by Sun and Mishima [24].

The comparison with Lazarek and Black [18] is shown in figure 8. On average, this model seems to be able to predict the experimental trend versus heat flux, while it strongly underpredicts the experimental results.

In figure 9 the experimental data are compared with predicted heat transfer coefficient values by Sun and Mishima [24] model. Sun and Mishima developed a new correlation based upon the Lazarek and Black [18] correlation and taking the effect of Weber number into account. This model is able to catch the experimental trend with heat flux but the data are underpredicted by 50%.

6. Conclusions

In the present paper the authors describe a different experimental technique to measure the flow boiling heat transfer coefficient in a square cross section microchannel having an hydraulic diameter of 1.23 mm, using a secondary fluid instead of fixing the heat flux by electrical heating.

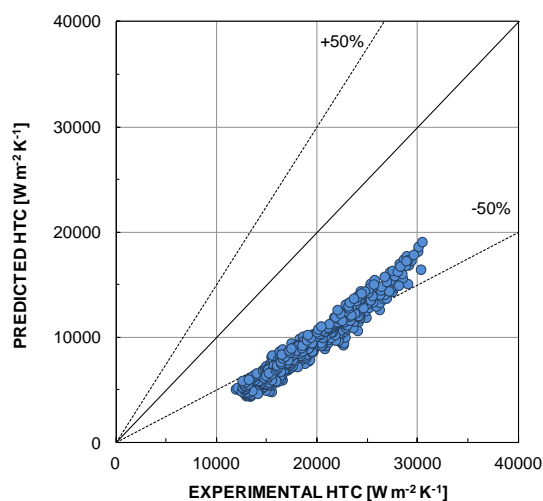


Figure 8. Experimental data compared against the model by Lazarek and Black [18].

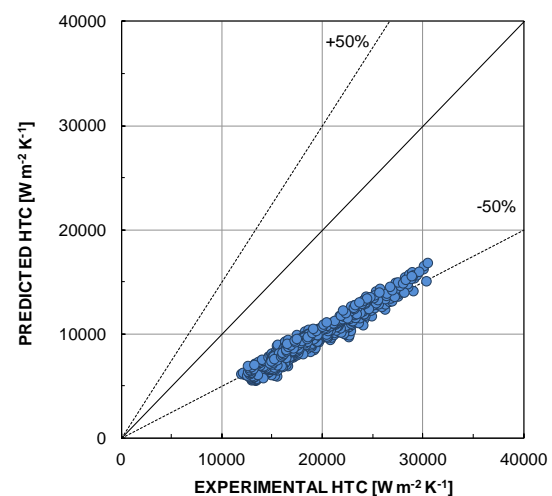


Figure 9. Experimental data compared against the model by Sun and Mishima [24].

The heat transfer coefficient is measured at around 30°C saturation temperature during flow boiling of R1234ze(E). The experimental heat transfer coefficient is highly dependent on the heat flux. The behavior of the heat transfer coefficients, that increase with heat flux in the saturated region, agrees with the results reported in the literature by many authors. Mass velocity and vapor quality were found to have a negligible effect on the heat transfer coefficient.

The present data is compared with R1234ze(E) flow boiling measurements by Del Col *et al.* [13] taken inside a 0.96 mm microchannel displaying a similar surface roughness. At the same experimental conditions (saturation pressure, mass velocity and heat flux), the heat transfer coefficient is higher in the square channel as compared to the circular one. It should be noticed that, the boiling process described in this paper and in the work by Del Col *et al.* [13] is governed by controlling the inlet temperature of the heating secondary fluid.

The present data has been compared with two predicting correlations available in the open literature: the model by Lazarek and Black [18] and the model by Sun and Mishima [24]. Both models are able to catch the heat transfer coefficient trend versus heat flux but none of them provides an accurate estimation of the heat transfer coefficients.

7. References

- [1] Thome J R, Bar-Cohen A, Revellin R and Zun I 2013 *Exp. Therm. Fluid Sci.* **44** 1-22
- [2] Chen L, Tian Y S and Karayiannis T G 2006 *Int. J. Heat and Mass Transfer* **49** 4220-4230
- [3] Tibiriçá C B and Ribatski G 2014 *Exp. Therm. Fluid Sci.* <http://dx.doi.org/10.1016/j.expthermflusci.2014.02.017>
- [4] Tibiriçá C B and Ribatski G 2013 *Int. J. Refrigeration* **36** 301-324
- [5] Bao Z Y, Fletcher D F and Haynes B S 2000 *Int. J. Heat and Mass Transfer* **43** 3347-3358
- [6] Tran T M, Wambuganss M W and France D M 1996 *Int. J. Multiphase Flow* **22** 485-498
- [7] Yan Y Y and Lin T F 1998 *Int. J. Heat and Mass Transfer* **41** 4183-4194
- [8] Lin S, Kew P A and Cornwell K 2001 *Int. J. Refrigeration* **24** 51-56
- [9] Ong C L and Thome J R 2004 *Exp. Therm. Fluid Sci.* **33** 651-663
- [10] Thome J R 2004 *Int. J. Heat and Fluid Flow* **25** 128-139
- [11] IPCC 2013 *Climate Change 2013: The Physical Science Basis. Contribution of Working Group I to the Fifth Assessment Report of the Intergovernmental Panel on Climate Change* ed Stocker T F, Qin D, Plattner G-K, Tignor M, Allen S K, Boschung J, Nauels A, Xia Y, Bex V and Midgley P M (Cambridge and New York: Cambridge University Press) p 733
- [12] Tibiriçá C B, Ribatski G and Thome J R 2012 *J. Heat Transfer* **134** 020906
- [13] Del Col D, Bortolato M and Bortolin S Measurements of heat transfer coefficient during flow boiling of two HFOs inside a circular minichannel, *Proc. 8th World Conference on Experimental Heat Transfer, Fluid Mechanics, and Thermodynamics* June 16-20 2013 Lisbon
- [14] Vakili-Farahani F, Agostini B and Thome J R 2013 *Int. J. Refrigeration* **36** 335-352
- [15] Del Col D and Bortolin S 2012 *Int. J. Thermal Sciences* **57** 25-36
- [16] Rawlings J O, Pantula S G and Dickey D A 1998 *Applied Regression Analysis* (New York: Springer)
- [17] Del Col D, Bisetto A, Bortolato M, Torresin D and Rossetto L 2013 *Int. J. Heat and Mass Transfer* **67** 326-337
- [18] Lazarek G M and Black S H 1982 *Int. J. Heat and Mass Transfer* **25** 945-960
- [19] Ong C L and Thome J R 2011 *Exp. Therm. Fluid Sci.* **35** 873-886
- [20] Del Col D, Bortolin S and Rossetto L 2013 *Int. J. Heat and Mass Transfer* **67** 1231-1245
- [21] Shiferaw D, Karayiannis T G and Kenning D B R 2009 *Int. J. Therm. Sci.* **48** 331-341
- [22] Maqbool M M, Palm B and Khodabandeh R 2013 *Exp. Therm. Fluid Sci.* **46** 120-130
- [23] Bortolin S, Da Riva E and Del Col D 2014 *Heat Transfer Engineering* **35** 193-203
- [24] Sun L and Mishima K 2009 *Int. J. Heat and Mass Transfer* **52** 5323-5329